IOSR Journal Of Pharmacy and Biological Sciences (IOSR-JPBS)
e-ISSN:2278-3008, p-ISSN:2319-7676. Volume 21, Issue 4 Ser. 1 (July. – August. 2026), PP 47-63
www.Iosrjournals.Org

Preparation, Characterization, And Evaluation Of Extracts Of Neem, Bitter Leaf And Scent Leaf As Aids In The Formulation Of A Triple Action Topical Herbal Cream

Obarisiagbon[1*] Aiwaguore Johnbull, Ekiseh[1] Miebi Ella, Onyenwe[2] Nathaniel Ejikeme, Omoregie[1] Augustina, Okunrobo[3] Mary, Airemwen[4] Ovenseri Collins

Department Of Pharmaceutics And Pharmaceutical Technology, College Of Pharmacy,Igbinedion University, Okada, Nigeria.
Department Of Pharmaceutical Microbiology, College Of Pharmacy, Igbinedion University, Okada, Nigeria.
Department Of Pharmacognosy, College Of Pharmacy, Igbinedion University, Okada, Nigeria.
Department Of Pharmaceutics And Pharamaceutical Technology, Faculty Of Pharmacy, Cyprus International University, Nicosia, Cyprus.

Abstract
Aim: *The increasing prevalence of antimicrobial resistance and the growing interest in plant-based therapeutic agents have stimulated this research into medicinal plants with potential pharmaceutical applications. It aimed to extract, characterize, and evaluate the antimicrobial properties of the ethanolic leaf extracts of Azadirachta indica (neem), Vernonia amygdalina (bitter leaf), and Ocimum gratissimum (scent leaf) which are widely used in traditional African medicine for the management of skin infections, wounds, and inflammatory conditions.*
Methods*: Fresh leaves of Neem, Bitter leaf and Scent leaf were collected from different farms in Okada community and authenticated with the Harberium numbers (IUO/11/024 for A. indica, IUO/16/022 for V. amygdalina, and IUO/13/068 for O. gratissimum) at the Department of Pharmacognosy. The leaves were air dried in a ventilated laboratory space for 7 days and milled using (Thomas Wiley Laboratory Mill, Model 4, Thomas Scientific, USA) to fine powder. Extraction was by maceration method using ethanol (96%) in a ratio of 1:2 plant powders to ethanol for 48 hours. The extracts were subjected to phytochemical, micromeritic and physicochemical characterization using Differential Scanning Calorimetry (DSC), X-ray Diffraction (XRD), Scanning Electron Microscopy (SEM) coupled with Energy Dispersive X-ray Analysis (SEM-EDX) studies. Triple action oil-in- water topical creams were formulated using different ratios of the extracts. Antimicrobial activities were studied against selected dermatological pathogens using standard microbiological procedures and their zones of inhibition were noted.*
Results*: Percentage yields of the extracts were neem (20.30), bitter leaf (17.30), and scent leaf (18.60). DSC analysis revealed that the extracts were thermally stable. XRD studies revealed amorphous characteristics and presence of minor crystalline mineral constituents. SEM-EDX analysis confirmed heterogeneous particle morphology with various elemental components. Micromeritic evaluation showed poor flow properties, as reflected by high Carr's Index and Hausner's ratio values. Antimicrobial studies demonstrated inhibitory activity of the extracts against selected pathogenic microorganisms, including Staphylococcus aureus and Candida albicans.*
Conclusion: *The research established that the ethanolic leaf extracts of A. indica, V. amygdalina, and O.gratissimum possess favorable physicochemical characteristics and significant antimicrobial activities, thereby providing scientific support for their traditional medicinal use.*
Keywords: *A.indica, V.amygdalina, O.gratissimum, Cream, Topical, Skin infections.*

Date of Submission: 11-07-2026 Date of Acceptance: 21-07-2026

I. Introduction

The skin is the largest organ of the human body and serves as the first line of defense against harmful microorganisms, chemicals, and other environmental factors. Besides its protective function, the skin is involved in temperature regulation, sensation, immune responses, and the prevention of excessive water loss. However, because of its constant exposure to the external environment, the skin is vulnerable to various

conditions such as wounds, burns, rashes, fungal infections, bacterial infections, eczema, and dermatitis. These skin disorders affect millions of people worldwide and can significantly reduce the quality of life of affected individuals (Kumar *et al*., 2020). The treatment of skin diseases often involves the use of topical formulations such as creams, ointments, gels, and lotions. Among these dosage forms, creams are particularly popular because they are easy to apply, spread smoothly on the skin, and are generally more acceptable to patients. Topical creams allow active ingredients to act directly at the site of infection or inflammation, thereby reducing systemic side effects and improving treatment outcomes (Aulton and Taylor, 2018). Over the years, synthetic antimicrobial and anti-inflammatory agents have been widely used in the treatment of skin-related infections and disorders. Although these products have proven effective, their continuous and excessive use has contributed to the growing problem of antimicrobial resistance. Many disease-causing microorganisms have developed resistance to commonly used drugs, making infections more difficult and expensive to treat. In addition, some synthetic topical preparations may cause adverse reactions such as skin irritation, allergic responses, dryness, and hypersensitivity in susceptible individuals (World Health Organization, 2023). These challenges have increased the search for safer, affordable, and more effective alternatives, particularly those derived from natural sources.

Medicinal plants have been used for centuries in traditional healthcare systems across the world. In many developing countries, including Nigeria, herbal medicine remains an important component of primary healthcare. The World Health Organization estimates that a large proportion of the world's population depends on medicinal plants for the prevention and treatment of diseases. The popularity of herbal medicine is largely due to its accessibility, affordability, cultural acceptance, and the belief that natural products are generally safer than synthetic drugs (WHO, 2023).

Among the numerous medicinal plants available in Nigeria, neem (*Azadirachta indica*), bitter leaf (*Vernonia amygdalina*), and scent leaf (*Ocimum gratissimum*) have gained considerable attention because of their extensive medicinal applications and proven pharmacological activities. These plants are readily available, relatively inexpensive, and widely used in traditional medicine for the treatment of various ailments.

Neem (*Azadirachta indica*) is one of the most valuable medicinal plants in tropical and subtropical regions. Often referred to as the "miracle tree" or "village pharmacy," neem has been used traditionally for the treatment of skin diseases, wounds, ulcers, infections, and inflammatory conditions. Various parts of the plant, including the leaves, seeds, bark, and roots, possess medicinal properties. Research has shown that neem contains several biologically active compounds such as azadirachtin, nimbin, nimbolide, flavonoids, and tannins. These compounds contribute to its antibacterial, antifungal, antiviral, anti-inflammatory, antioxidant, and wound-healing effects (Subapriya and Nagini, 2005). Due to these properties, neem has become an important plant in the development of herbal products for skin care and disease management.

Bitter leaf (*Vernonia amygdalina*) is another medicinal plant widely used throughout Africa. Apart from its use as a vegetable, bitter leaf has long been utilized in traditional medicine for the treatment of malaria, gastrointestinal disorders, infections, and inflammatory diseases. Scientific studies have identified several phytochemicals in bitter leaf, including flavonoids, alkaloids, tannins, saponins, and sesquiterpene lactones. These compounds have been reported to possess antimicrobial, antioxidant, anti-inflammatory, and immune-enhancing activities (Farombi and Owoeye, 2011). The antimicrobial properties of bitter leaf make it particularly useful in combating microorganisms associated with skin infections and wound contamination. Similarly, scent leaf (*Ocimum gratissimum*) is an aromatic medicinal plant commonly found in many parts of Nigeria. It is widely used in traditional medicine for treating skin infections, respiratory illnesses, gastrointestinal disorders, and fever. The plant contains essential oils rich in eugenol, thymol, and other phenolic compounds that exhibit strong antimicrobial and antioxidant activities. Several studies have demonstrated that extracts of scent leaf are effective against both Gram-positive and Gram-negative bacteria as well as certain fungal pathogens (Prabhu *et al*., 2009). Its antiseptic and anti-inflammatory properties further support its potential use in topical formulations.

The individual therapeutic benefits of neem, bitter leaf, and scent leaf have been well documented. However, recent research has shown that combining different medicinal plants in a single formulation may produce synergistic effects. Synergy occurs when the combined action of different plant extracts produces greater therapeutic benefits than when each extract is used alone. By combining neem, bitter leaf, and scent leaf, it may be possible to develop a topical cream with enhanced antimicrobial, anti-inflammatory, antioxidant, and wound-healing properties. Such a formulation could provide broader therapeutic coverage against various skin conditions while utilizing naturally available resources.

A properly formulated cream can improve the stability of active ingredients, ensure consistent dosage, enhance patient convenience, and increase the overall effectiveness of the treatment. The formulation of a topical herbal cream requires careful consideration of both active ingredients and formulation excipients. Furthermore, the quality of the final product must be assessed through physicochemical evaluations such as pH determination, viscosity measurement, spreadability testing, homogeneity assessment, appearance evaluation,

and stability studies. These parameters are essential for ensuring that the cream remains safe, effective, and acceptable throughout its shelf life (Aulton and Taylor, 2018). Therefore, this study is undertaken to formulate and evaluate a topical herbal cream using extracts of neem (*Azadirachta indica*), bitter leaf (*Vernonia amygdalina*), and scent leaf (*Ocimum gratissimum*). The study seeks to determine the suitability of these plant extracts for incorporation into a cream formulation and to evaluate the physicochemical characteristics of the formulated product. Ultimately, the research is expected to contribute to the growing interest in herbal medicine and provide scientific evidence supporting the use of locally available medicinal plants in the development of topical pharmaceutical preparations.

II. Methodology

The theoretical framework underpinning this study is rooted in the science of pharmaceutical formulation, ethnopharmacology, and phytochemistry. This research integrates knowledge from these disciplines to rationally design, develop, and evaluate a topical herbal cream incorporating extracts of neem (*Azadirachta indica*), bitter leaf (*Vernonia amygdalina*), and scent leaf (*Ocimum gratissimum*). The theoretical basis of this study draws on three major frameworks: (1) the biopharmaceutical theory of topical drug delivery, (2) the pharmacognostic and phytochemical basis of herbal drug activity, and (3) the concept of synergistic phytotherapy.

The study was conducted in three sequential phases: (1) plant material collection, authentication, and preparation; (2) extraction and phytochemical screening; and (3) cream formulation, optimization, and evaluation.

III. Materials

Plant Materials

Fresh leaves of *Azadirachta indica* A. Juss (neem), *Vernonia amygdalina* Delile (bitter leaf), and *Ocimum gratissimum* L. (scent leaf) were collected in the early morning hours (between 7:00 and 9:00 a.m.) from different farms in Okada community, Edo state, Nigeria, in the month of June. The time of collection was chosen to minimize photochemical degradation and to capture peak secondary metabolite content, as early-morning collection after overnight accumulation is associated with higher concentrations of volatile and non-volatile phytoconstituents (Ncube *et al*., 2022). Botanical identification and authentication of the three plant species were carried out at the Department of Pharmacogonsy. Voucher specimens were deposited in the Pharmacognosy Herbarium, College of Pharmacy, Igbinedion University, Okada (Voucher Numbers: Iuo/11/042 for *A. indica*; Iuo/16/022 for *V. amygdalina*; Iuo/13/068 for *O. gratissimum*) for future reference, in compliance with the recommendations of the International Plant Names Index and established pharmacognostic authentication protocols (Naikwadi and Bhise, 2023).

Chemicals and Reagents

All chemicals and reagents used were of analytical grade unless otherwise stated. The following were procured from Sigma-Aldrich (St. Louis, MO, USA), BDH Chemicals Ltd. (Poole, UK), or May & Baker Ltd. (Dagenham, UK): ethanol (95%), methanol (analytical grade), chloroform, n-hexane, distilled water (freshly prepared), Dragendorff's reagent, Mayer's reagent, Wagner's reagent, Fehling's solution A and B, ferric chloride ($FeCl_3$, 1% w/v solution), lead acetate solution, concentrated H_2SO_4, concentrated HCl, Folin–Ciocalteu reagent, gallic acid, quercetin, sodium carbonate, aluminium chloride, sodium nitrite, sodium hydroxide, 2,2-diphenyl-1-picrylhydrazyl (DPPH) radical, ascorbic acid, Muller–Hinton agar (MHA), Muller–Hinton broth (MHB), sabouraud dextrose agar (SDA), dimethyl sulphoxide (DMSO), and McFarland turbidity standards.

Equipment and Apparatus

Analytical balance (Mettler Toledo, XSE205, Switzerland, sensitivity ± 0.01 mg); Rotary evaporator (Buchi R-210, Germany); Digital pH meter (Hanna Instruments HI 2211, USA, calibrated with standard buffers of pH 4.0 and 7.0); Brookfield viscometer model DV-II+ Pro (Brookfield Engineering Laboratories, Middleboro, MA, USA); Digital vernier callipers; Cone and plate viscometer; Thermostatic water bath (Grant Instruments GD120); Oven (Memmert UN55); Autoclave (HiClave HVE-50); Laminar air flow cabinet (Biobase BSC-1300IIA2); Colony counter; UV-visible spectrophotometer (Shimadzu UV-1900, Japan); Hot plate magnetic stirrer (Hesidolph MR Hei-Standard); Microscope (Olympus CX23, Japan); Homogeniser (IKA T25 Ultra-Turrax, Germany); Franz diffusion cell apparatus; Centrifuge (Eppendorf Centrifuge 5810R).

Preparation of plant material

Freshly harvested leaves of the three plant species were gently washed under running tap water to remove surface dirt, dust, and extraneous matters, followed by a final rinse with distilled water to remove any residual tap water contaminants. The washed leaves were spread on clean stainless-steel trays and air-dried

under shade at ambient temperature (25–30°C) for a period of 14 days. Shade drying was preferred over oven drying to minimize the thermal degradation of heat-labile phyto-constituents, particularly terpenoids and volatile phenolics, which are known to be susceptible to temperatures above 40°C (Azwanida, 2015; Ncube *et al*., 2022). The dried leaves were subsequently pulverized into a coarse powder using a stainless-steel laboratory mill

(Thomas Wiley Mill, Model 4, USA) fitted with a 0.5 mm mesh sieve and stored in amber-colored glass bottles sealed with airtight lids at room temperature until further use.

Determination of Moisture Content

The moisture content of the powdered plant materials was determined gravimetrically. Accurately weighed portions (2 g) of each powdered sample were placed in pre-weighed crucibles and dried in a hot air oven at 105°C for 3 hours until a constant weight was achieved. Moisture content was calculated using the formula:

Moisture Content (%) = $\frac{w1-w2}{w1} \times 100$ ---------- 1

Where, W_1 is the initial weight of the powdered sample and W_2 is the weight after drying. A moisture content of less than 8% was accepted as the criterion for adequate drying, in accordance with WHO quality standards for herbal drugs (World Health Organization, 2019; Edeoga *et al*., 2020).

Preparation of ethanol extracts

Ethanol extraction was employed as the primary extraction solvent system based on ethanol's (95% v/v) broad-spectrum solvation capacity for both polar and moderately non-polar phyto-constituents. Ethanol has a Generally Recognized As Safe (GRAS) status, its capacity to serve as a preservative, and its wide application in the preparation of standardized herbal extracts intended for pharmaceutical formulations (Mandal *et al*., 2021) as reviewed by Pandey and Tripathi, 2022). Maceration was selected as the extraction method. Each powdered plant material (200 g) was macerated in 1,000 mL of 95% ethanol in a closed conical flask at room temperature (25 ± 2°C) with intermittent shaking for 72 hours. This cold maceration method was preferred over Soxhlet extraction or decoction to preserve thermolabile bioactive constituents and obtain a broader phytochemical profile (Azwanida, 2015). After maceration, the extract was filtered through a double layer of Whatman No. 1 filter paper (Whatman International Ltd., Maidstone, UK) and subsequently through a 0.45 µm membrane filter to remove particulate matter. The filtrates were concentrated under reduced pressure at 40°C using a rotary evaporator (Buchi R-210) until a semi-solid mass was obtained. The concentrated extract was then transferred to pre-weighed evaporating dishes and placed in a thermostatically controlled water bath set at 40°C to complete the drying and also remove residual solvent. The dried extracts were scraped from the evaporating dishes, weighed, and stored in sealed amber glass vials at 4°C until use.

Percentage yield of extracts

The percentage yield of each extract was calculated using the formula:

yield of extract (%) = $\frac{weight\ of\ dried\ extract}{weight\ of\ powdered\ plant\ material} \times 100$ ---------- 2

Phytochemical screening: Qualitative phytochemical screening of the crude ethanolic extracts of the three plants were performed to detect the presence of major classes of secondary metabolites using standard colorimetric, precipitation, and foam tests as described by Trease and Evans (2022) and Harborne (2019). The phytochemical tests for alkaloids, flavonoids, tannins, saponins, terpenoids, steroids and cardiac glycosides were performed.

Evaluation of extracts: The extracts were subjected to a series of carefully selected evaluation tests. The goal was to determine whether they actually met the quality, safety, and performance standards expected of a topical pharmaceutical product. Because these extracts bring together three botanically rich plant extracts, each contributing its own complex mixture of phytochemicals, it was particularly important to evaluate not just the physical appearance of the cream, but also how stable it was, how it behaved on the skin, and whether the active plant constituents remained intact and evenly distributed throughout the formulation. The evaluation was therefore organized into two broad sections: standard physicochemical and micromeritic characterization, and advanced instrumental analysis.

Macromeritic characterization of powdered plant extracts.

Bulk density: Bulk density was determined by carefully pouring a known weight of each powder (m) into a dry graduated measuring cylinder without compaction and recording the volume occupied (V_0). The bulk density was calculated as:

Bulk density = $\frac{m}{V0}$ ---------- 3

Tapped density: Tapped density was determined using the same powder sample after subjecting it to 100 taps using a calibrated tap density tester (Electrolab ETD-1020), in accordance with USP <616> (USP, 2023). Tapped density was calculated as:

Tapped density = $\frac{m}{Vt}$ ---------- 4

Carr's compressibility index: Once bulk and tapped density values were obtained, Carr's compressibility index (CI) was calculated using the expression:

Compressibility index (%) = [(tapped density – bulk density) / tapped density] × 100 --------

Hausner's ratio: Hausner's ratio was calculated from the following relationship:

Hausner's ratio = $\frac{\text{tapped density}}{\text{bulk density}}$ ---------- 5

Angle of repose: Angle of repose was determined using the fixed funnel method: each powder weight was allowed to flow freely through a funnel held at a fixed height above a flat surface, forming a conical heap. The angle (θ) was calculated as:

Tan θ = $\frac{h}{r}$ ---------- 6

Where, h is the height of the powder cone and r is the radius of the base. An angle of ≤30° indicates excellent flow, 31–40° is acceptable, 41–50° is poor, and > 50° is very poor flow (Lachman *et al*., 2013)

Particle size and size distribution: Particle size analysis was carried out using laser diffraction (Malvern Mastersizer 3000, UK), with each dried extract dispersed in an appropriate non-reactive liquid medium. The volume-weighted mean diameter D [4, 3] and the cumulative percentile values D10, D50, and D90 were recorded. The breadth of the size distribution was expressed using the span:

Span = $\frac{D90-D10}{D50}$ ---------- 7

A high span value indicates a wide, polydispersed distribution, meaning the powder contains a broad mixture of fine and coarse particles which shows how well the plant extract disperses within the cream base. Very coarse particles may not disperse fully during emulsification, leading to a gritty texture that patients would find unpleasant on the skin. The ideal is a reasonably narrow, consistent distribution.

Porosity and true density: True density which is the actual density of the solid material (excluding any pores or void spaces) was measured by helium pycnometry (AccuPyc II 1340, Micromeritics Instrument Corporation). From this, the porosity of the powder bed was estimated as:

Porosity (%) = 1- $\frac{bulk\ density}{true\ density}$ × 100 ---------- 8

For freeze-dried or spray-dried herbal extracts, porosity values tend to be relatively high because of the porous internal structure created during the drying process. While this can cause poor flow, the same porous structure also provides a high surface area that aids in the dissolution and release of phytochemicals once the cream is applied to the skin

X-Ray Powder Diffractometry (XRPD): X-ray powder diffraction (XRPD) was carried out using a PANalytical X'Pert PRO diffractometer with CuKα radiation (λ = 1.5406 Å), operating at 45 kV and 40 mA. The samples analysed included the individual freeze-dried plant extracts, the excipients used in the cream base (cetyl alcohol, beeswax, Tween 80), and the lyophilized final cream formulation.

Scanning Electron Microscopy with Energy-Dispersive X-ray Spectroscopy (SEM-EDX):

SEM-EDX analysis was performed using a JEOL JSM-7600F field-emission scanning electron microscope equipped with an Oxford Instruments EDX detector.

Differential Scanning Calorimetry (DSC): DSC analy**sis** was conducted using a TA Instruments DSC Q2000, calibrated with indium (melting point 156.6°C; ΔH = 28.45 J/g) to ensure temperature and enthalpy accuracy. The samples analyzed included the pure dried extracts, individual excipients, physical mixtures of extracts with excipients, and the lyophilized cream formulation.

Antimicrobial evaluation of crude extracts: Antimicrobial activity of the three crude ethanolic plant extracts was evaluated at the preformulation stage against two clinically relevant test organisms selected on the basis of their significance in dermatological and superficial infections: Staphylococcus *aureus* ATCC 25923 (a Gram-positive bacterium and the leading causative agent of skin and soft tissue infections, impetigo, folliculitis, and wound infections in sub-Saharan Africa) and Aspergillus niger (a filamentous fungus associated with superficial

mycoses, onychomycosis, and opportunistic skin infections, particularly in tropical climates) (Ogunjimi *et al*., 2022). These two organisms were selected to reflect the dual antibacterial–antifungal therapeutic scope of the planned triple-action cream.

Preparation of test organisms: Staphylococcus aureus ATCC 25923 was obtained as a certified reference strain from the ATCC and maintained on Mueller–Hinton Agar (MHA) slants at 4°C with monthly sub-culturing. Aspergillus niger was sourced from the Microbiology Laboratory of the College of Pharmacy, where it was maintained on Sabouraud Dextrose Agar (SDA) at room temperature. Prior to use, S. aureus was cultured in Mueller–Hinton Broth (MHB) at 37°C for 18–24 hours and the resulting suspension adjusted to a turbidity equivalent to 0.5 McFarland standard (approximately 1.5×10^8 CFU/mL) using the UV-visible spectrophotometer at 625 nm. A. niger spore suspensions were prepared by flooding mature SDA plate cultures with sterile normal saline containing 0.05% Tween 80 and adjusted to 1.0×10^6 spores/mL using a haemocytometer.

Agar well diffusion assay:

Antimicrobial activity was assessed by the agar well diffusion method following the Clinical and Laboratory Standards Institute (CLSI, 2022) guidelines. Standardized *S. aureus* inoculum was spread uniformly on MHA plates using sterile swabs. *A. niger* spore suspensions were spread on SDA plates. Wells of 6 mm diameter were bored into the agar surface using a sterile cork borer and filled with 100 µL of each extract solution (200 mg/mL in DMSO: distilled water, 1:1 v/v). Ciprofloxacin disc (5 µg) was used as the positive antibacterial control and fluconazole disc (25 µg) as the positive antifungal control; DMSO: distilled water (1:1) served as the negative control. Plates were pre-incubated at 4°C for 2 hours to allow prediffusion of the test substances before incubation at 37°C for 24 hours (*S. aureus*) and 28°C for 48–72 hours (*A. niger*). Zones of inhibition (including the well diameter) were measured in millimeters using a digital vernier caliper. All experiments were performed in triplicate and results expressed as mean ± SD.

Minimum inhibitory concentration (MIC) determination*:* Minimum inhibitory concentration (MIC) of each extract against *S. aureus* and *A. niger* was determined using the broth micro dilution method in accordance with CLSI (2022) M07-A12 guidelines. Serial two-fold dilutions of each extract were prepared in 96-well flat-bottomed microliter plates in MHB (for *S. aureus*) and Sabouraud Dextrose Broth (SDB) (for *A. niger*), covering a concentration range of 0.078 – 10 mg/mL. Each well was inoculated with the standardized microbial suspension and the plates incubated as described above. After incubation, 20 µL of 0.5% triphenyltetrazolium chloride (TTC) solution was added to each well as a viability indicator. The MIC was defined as the lowest concentration of the test substance that completely inhibited visible microbial growth. Ciprofloxacin and fluconazole were used as reference antimicrobials. All experiments were performed in triplicate on three separate occasions.

Statistical analysis: All data were expressed as mean ± standard deviation (SD) from triplicate determinations. Statistical analysis was performed using IBM SPSS Statistics version 29.0 (IBM Corp., Armonk, NY, USA). One-way analysis of variance (ANOVA) was used to compare means across the three plant extract groups, followed by Tukey's Honest Significant Difference (HSD) post-hoc test for pairwise multiple comparisons. Pearson's correlation coefficient was used to assess associations between phytochemical content and biological activity (antimicrobial zones of inhibition, MIC values, and DPPH IC_{50}). Statistical significance was set at $p < 0.05$ for all tests (Bhattacharyya, 2021; Motulsky, 2021).

IV. Results And Discussion

Results of % yield of the three plants extracts are presented in Table 1, neem leaf (20.30), bitter leaf (17.60), scent leaf (18.60). The % yield of neem aligns with its well-documented richness in limonoids, flavonoids, and other soluble terpenoids (Siddiqui *et al*., 2022). Bitter leaf and scent leaf yields are consistent with earlier reports for ethanolic extractions (Onwudiwe *et al*., 2023; Khalil *et al*., 2022). Ethanol was selected as the extraction solvent because of its ability to dissolve both polar and moderately non-polar phytochemical classes, including phenolic acids, flavonoids, alkaloids, and terpenoids, thereby maximizing recovery of bioactive materials (Azwanida, 2015; Pandey and Tripathi, 2014). Together, the yield values are considered satisfactory and support the suitability of these extracts for incorporation into a topical cream formulation with combined antimicrobial, anti-inflammatory, and wound-healing activity (Elufioye *et al*., 2021).

Differential Scanning Calorimetry (DSC)

Differential Scanning Calorimetry is a widely used thermoanalytical method in pharmaceutical research that monitors the heat flow into or out of a sample as it is heated at a controlled rate.

The analysis was carried out on the plant extracts using a Mettler Toledo STAR System (SW 13.00) under nitrogen purge, heating from 40°C to 240°C at a rate of 10°C/min.

The DSC thermogram of Sample A - the bitter leaf extracts (Figure 4.1) - displays a distinctly different thermal profile compared to the other two extracts. The curve begins with a very sharp, steep endothermic spike immediately from 40°C, which rapidly descends to approximately −2.5 mW by 60°C. This pronounced early event is indicative of a high residual moisture content and the loss of tightly bound water molecules from the hygroscopic extract matrix - consistent with the nitrogen-rich, urea-type composition identified in the XRPD analysis, as urea-type compounds are known to interact strongly with water and release it in a sharp endothermic event upon heating (Onwudiwe *et al*., 2023; Ruggiero *et al*., 2023). The curve then plateaus at approximately −3.0 mW between 80 and 120°C, forming a broad endothermic shoulder, before showing a moderate endothermic trough at approximately 130°C. This event is broader and occurs at a lower temperature than the corresponding troughs in Samples B and C, reflecting the lower content of high-melting crystalline limonoid and silica-related phases in bitter leaf. Beyond 140°C, the heat flow recovers gradually and the thermogram becomes relatively flat between 160 and 240°C, with no sharp secondary transitions, suggesting that the majority of thermally active constituents have undergone their transitions by 140°C. The absence of any exothermic events confirms the thermal stability of the bitter leaf extract within the temperature range relevant to cream preparation and storage (Mura *et al*., 2022; Adetunji *et al*., 2021).

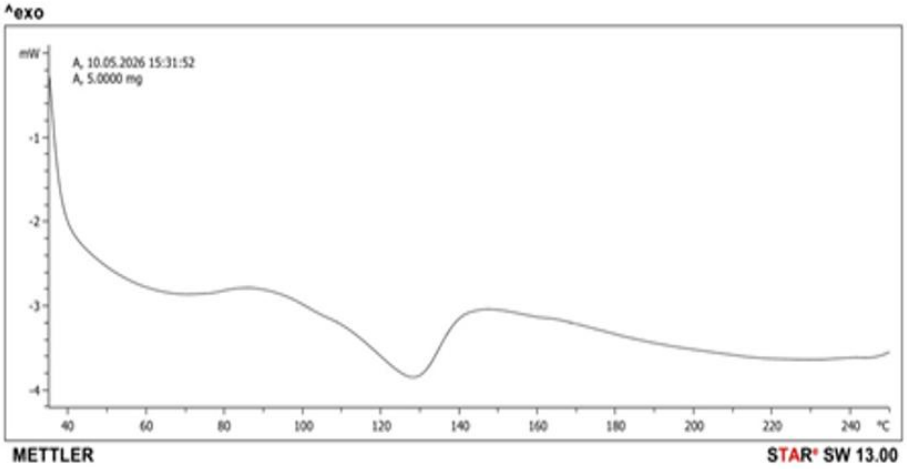

Figure 4.1: DSC Thermogram of Sample A (Bitter leaf extract).

Looking at the thermogram for Sample B the neem leaf extract (Figure 4.2) the curve begins with a broad, gradual endothermic shift between 40 and 80°C. This early thermal event is typical of moisture evaporation and dehydration of the extract matrix, and is commonly observed in complex, hygroscopic plant-derived materials (Ruggiero *et al*., 2023). As the temperature rises toward 155°C, a sharp and well-defined endothermic trough appears, reaching a heat flow of approximately 6.8 mW. This peak is attributed to the melting of crystalline constituents within the neem extract, most likely nimbidin and related limonoid compounds, whose thermal behavior falls within this temperature range (Siddiqui *et al*., 2022).

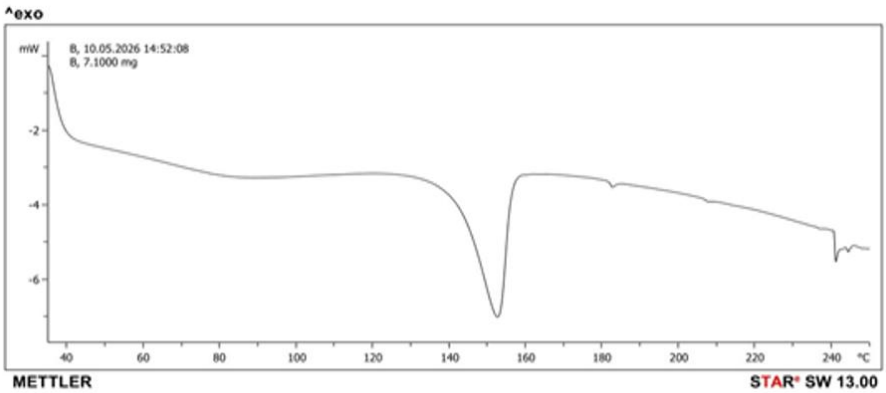

Figure 4.2. DSC Thermogram of Sample B (Neem leaf extract).

The thermogram for Sample C - scent leaf extract (Figure 4.3) follows a broadly similar pattern. A relatively wide endothermic region between 40 and 80°C again reflects the loss of bound and residual moisture from the extract. This thermal event is consistent with the melting of eugenol-containing crystalline fractions and flavonoid glycosides that are characteristic of *Ocimum gratissimum* (Khalil *et al*., 2022).

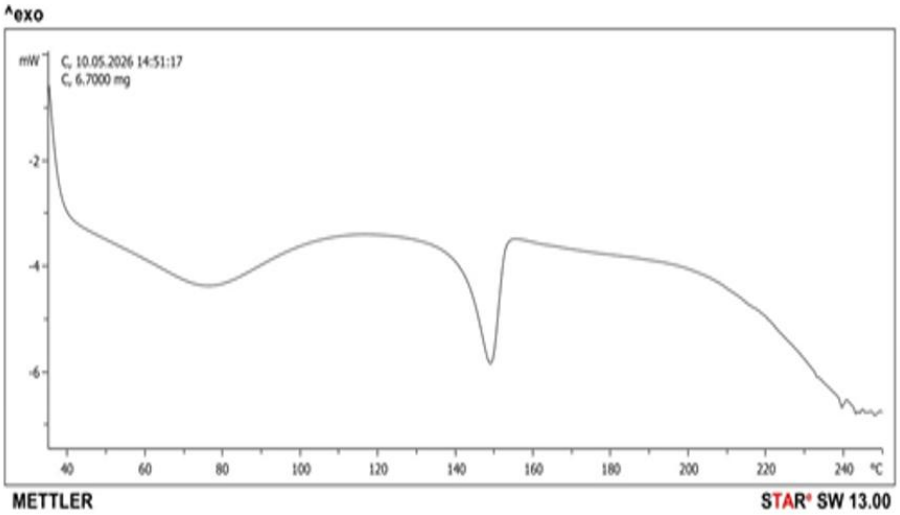

Figure 4.3. DSC Thermogram of Sample C (Scent leaf extract)

X-Ray Powder Diffraction (XRPD) Analysis

X-ray powder diffraction is a non-destructive analytical technique that exploits the characteristic diffraction patterns produced when X-rays interact with the crystalline planes of a solid material. Each crystalline phase produces a unique pattern of peaks at defined 2θ angles effectively a fingerprint that can be matched against reference databases for qualitative and quantitative phase identification (Chauhan *et al*., 2020).

The diffractogram of Sample A - bitter leaf extract (Figures 4 and 5) was dominated by low-intensity, broad humps spread across the 2θ range of 10–60°, a pattern that is characteristic of a predominantly amorphous material. The substantial presence of the urea phase is not unexpected, since bitter leaf contains an unusually high proportion of nitrogen-containing metabolites and protein-bound nitrogen, some of which adopt urea-like crystal structures upon drying (Onwudiwe *et al*., 2023). Cristobalite is a silica polymorph that arises from the silica phytoliths naturally deposited within the leaf tissue of many plant species (Ndukwe *et al*., 2021).

Sylvite (KCl) is consistent with the well-documented potassium richness of *Vernonia amygdalina* (Farombi and Owoeye, 2011; Onwudiwe *et al*., 2023).

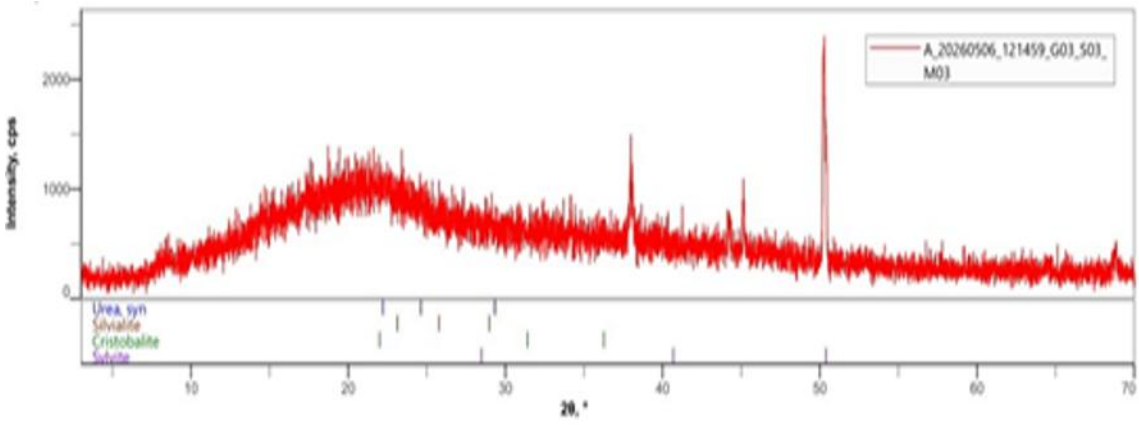

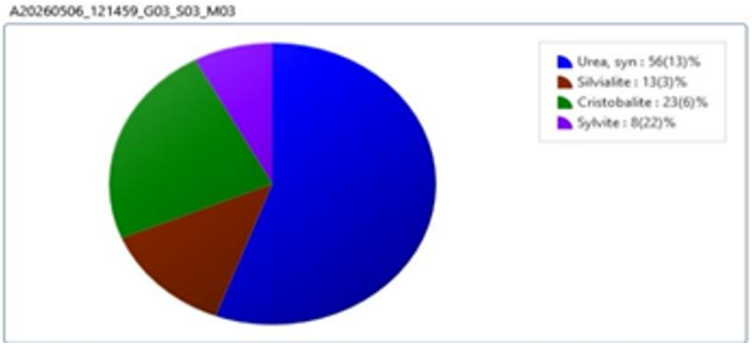

Figure 4. XRD quantitative analysis report – Sample A (Bitter leaf extract).

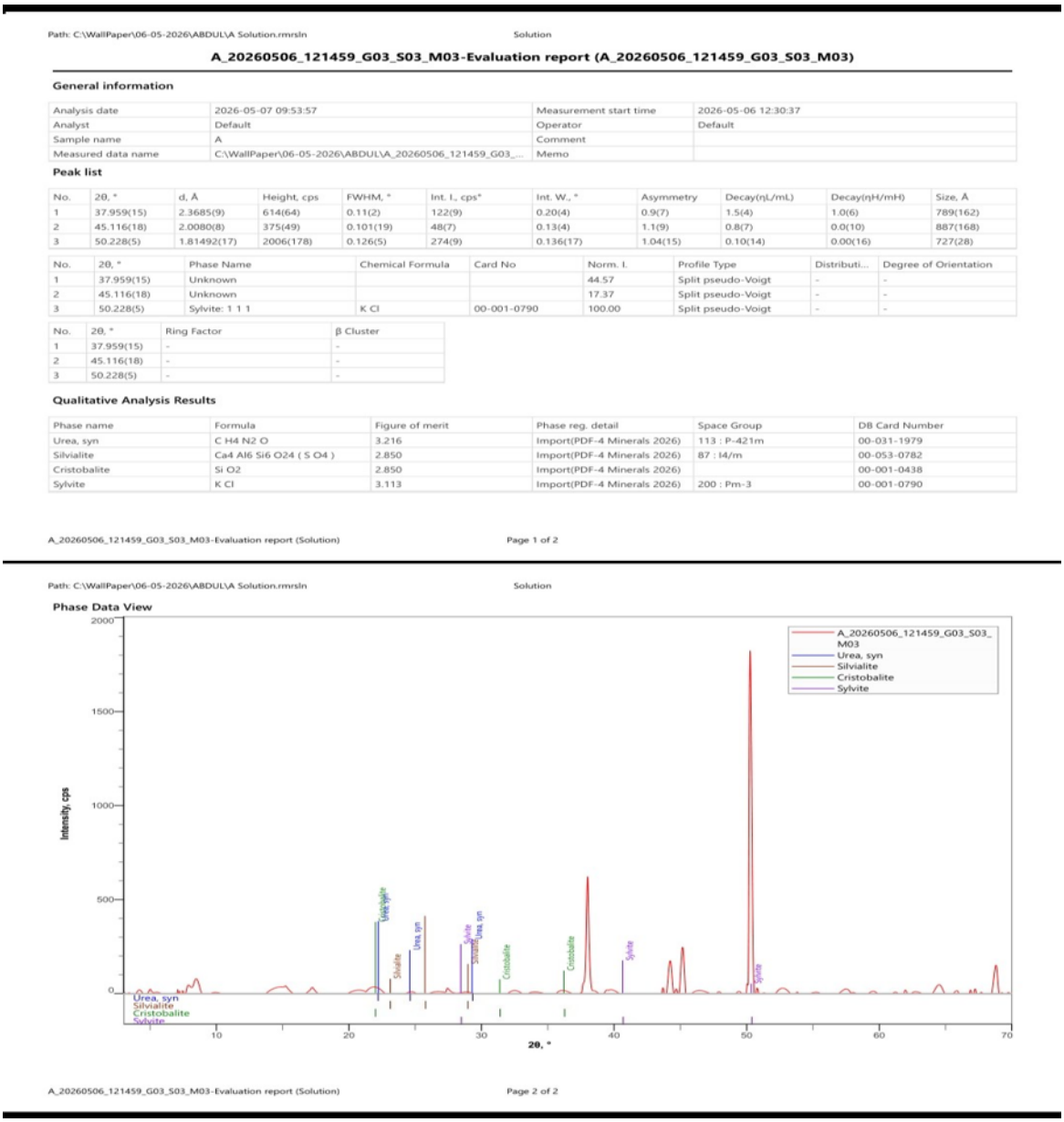

Path: C:\WallPaper\06-05-2026\ABDUL\A Solution.rmrsln Solution

A_20260506_121459_G03_S03_M03-Evaluation report (A_20260506_121459_G03_S03_M03)

General information

Analysis date	2026-05-07 09:53:57	Measurement start time	2026-05-06 12:30:37
Analyst	Default	Operator	Default
Sample name	A	Comment	
Measured data name	C:\WallPaper\06-05-2026\ABDUL\A_20260506_121459_G03_...	Memo	

Peak list

No.	2θ, °	d, Å	Height, cps	FWHM, °	Int. I., cps*	Int. W., °	Asymmetry	Decay(η)L/mL)	Decay(η)H/mH)	Size, Å
1	37.959(15)	2.3685(9)	614(64)	0.11(2)	122(9)	0.20(4)	0.9(7)	1.5(4)	1.0(6)	789(162)
2	45.116(18)	2.0080(8)	375(49)	0.101(19)	48(7)	0.13(4)	1.1(9)	0.8(7)	0.0(10)	887(168)
3	50.228(5)	1.81492(17)	2006(178)	0.126(5)	274(9)	0.136(17)	1.04(15)	0.10(14)	0.00(16)	727(28)

No.	2θ, °	Phase Name	Chemical Formula	Card No	Norm. I.	Profile Type	Distributi...	Degree of Orientation
1	37.959(15)	Unknown			44.57	Split pseudo-Voigt	-	-
2	45.116(18)	Unknown			17.37	Split pseudo-Voigt	-	-
3	50.228(5)	Sylvite: 1 1 1	K Cl	00-001-0790	100.00	Split pseudo-Voigt	-	-

No.	2θ, °	Ring Factor	β Cluster
1	37.959(15)	-	-
2	45.116(18)	-	-
3	50.228(5)	-	-

Qualitative Analysis Results

Phase name	Formula	Figure of merit	Phase reg. detail	Space Group	DB Card Number
Urea, syn	C H4 N2 O	3.216	Import(PDF-4 Minerals 2026)	113 : P-421m	00-031-1979
Silvialite	Ca4 Al6 Si6 O24 (S O4)	2.850	Import(PDF-4 Minerals 2026)	87 : I4/m	00-053-0782
Cristobalite	Si O2	2.850	Import(PDF-4 Minerals 2026)		00-001-0438
Sylvite	K Cl	3.113	Import(PDF-4 Minerals 2026)	200 : Pm-3	00-001-0790

A_20260506_121459_G03_S03_M03-Evaluation report (Solution) Page 1 of 2

Path: C:\WallPaper\06-05-2026\ABDUL\A Solution.rmrsln Solution

Phase Data View

A_20260506_121459_G03_S03_M03-Evaluation report (Solution) Page 2 of 2

Figure 5. XRD evaluation report – Sample A (Bitter leaf extract).

Sample B - neem leaf extract (Figures 6 and 7) yielded the most complex diffraction profile of the three extracts. The evaluation report identified a single definitively assignable peak at 2θ = 20.81° (d = 4.266 Å; crystallite size ~5.41 Å), assigned to synthetic urea (Card No. 00-031-1979), while the remainder of the diffraction pattern resisted confident assignment, confirming this extract is overwhelmingly amorphous. Five

phases were tentatively resolved: Cristobalite 31(36) wt%, Marialite 22(51) wt%, Urea, syn 16(28) wt%, Graphite 21(44) wt%, and Sylvite 9(26) wt%. The apparent graphite-like, most likely arises from the dense condensed aromatic ring systems found in neem's polyphenolic fraction (Siddiqui *et al*., 2022). Marialite reflects trace aluminosilicate impurities within the leaf tissue. The very high uncertainty values across all phases underscore the amorphous nature of this extract (Chauhan *et al*., 2020).

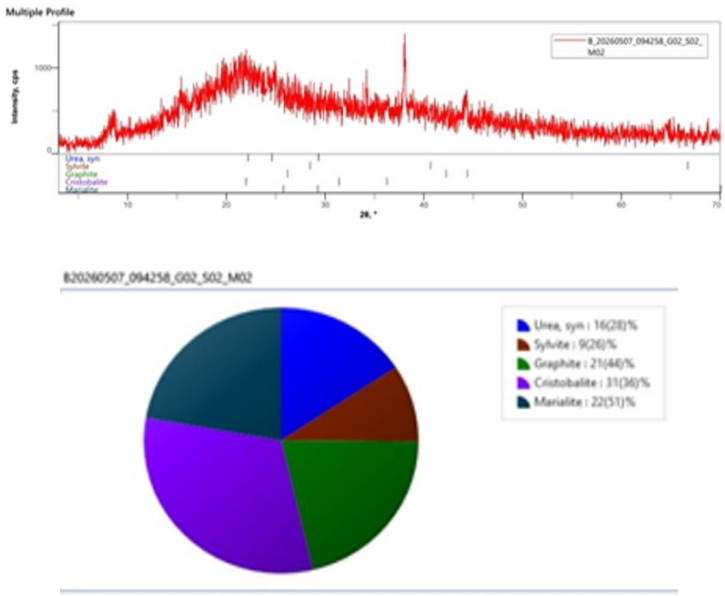

Figure 6. XRD quantitative analysis report – Sample B (Neem leaf extract)

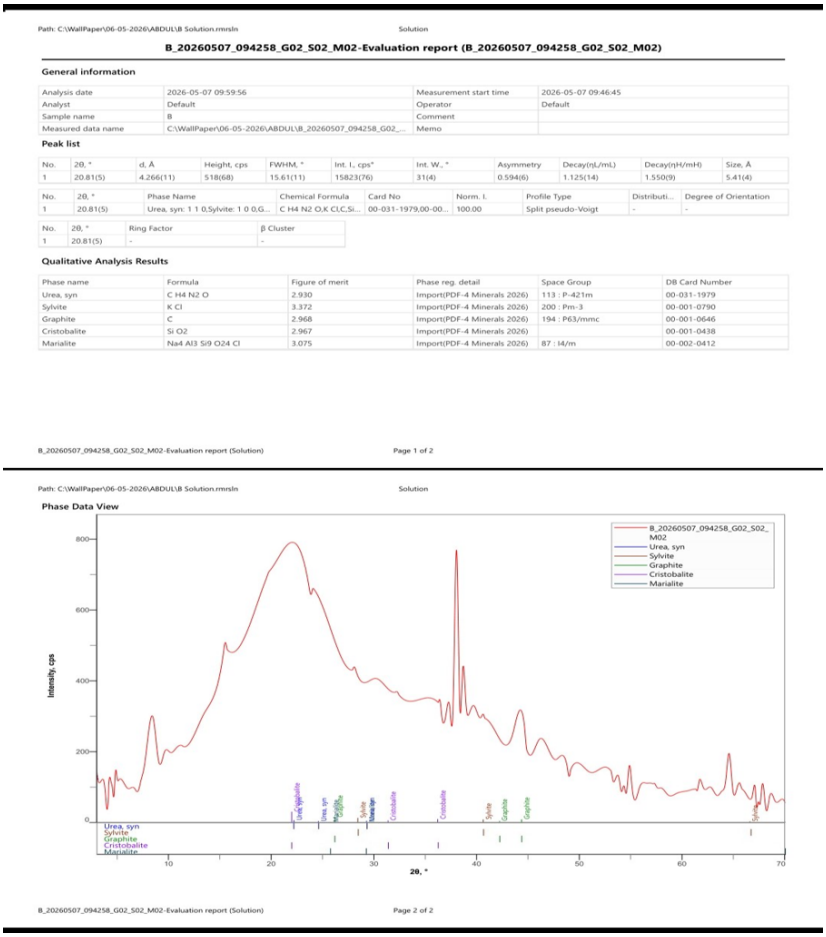

Figure 7. XRD evaluation report–Sample B (Neem leaf extract)

Sample C - Scent leaf extract (Figures 8 and 9) stood out clearly from the other two extracts by displaying the sharpest and most clearly defined diffraction peaks, indicating significantly higher crystallinity. Thirteen distinct peaks were resolved, with the strongest reflection at $2\theta \approx 26.82°$ (d = 3.221 Å, normalized intensity = 100.00), corresponding to the primary reflection of quartz. Quantitative phase analysis confirmed quartz (Card No. 04-027-5352) as the dominant phase at 64(4) wt%, with orthoclase 22(3) wt%, illite 11(3) wt%, and albite 3(3) wt%. The dominance of Quartz is consistent with published reports showing that Lamiaceae family members are particularly efficient silica accumulators (Ndukwe *et al*., 2021; Chauhan *et al*., 2020). Feldspar-group minerals (orthoclase and albite) and illite most likely represent residual soil-derived mineral fraction in the plant material. The relatively low uncertainty for all four phases especially quartz at ±4 wt% confirms a reliable quantitative result.

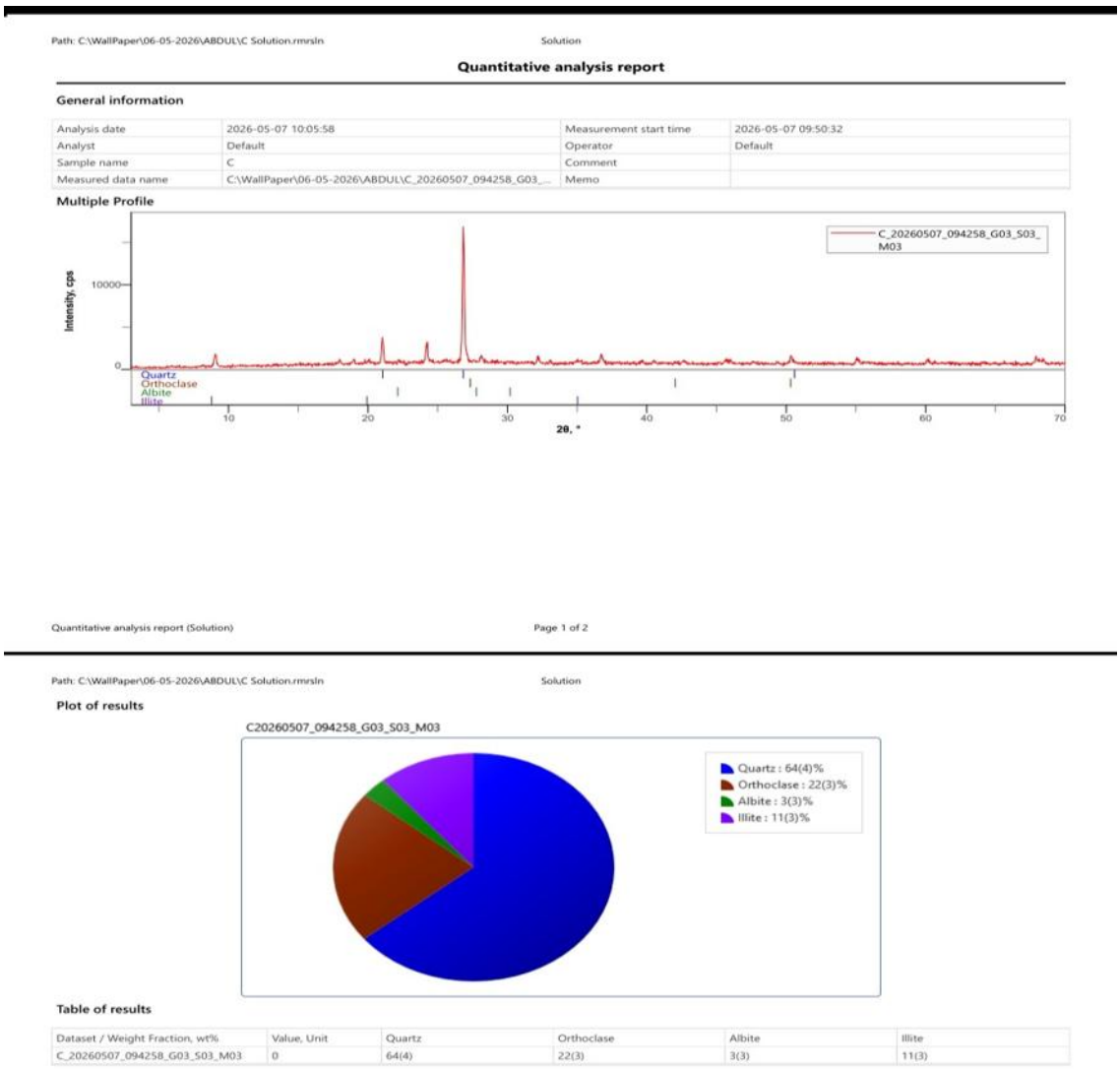

Figure 8. XRD quantitative analysis report – Sample C (Scent leaf extract)

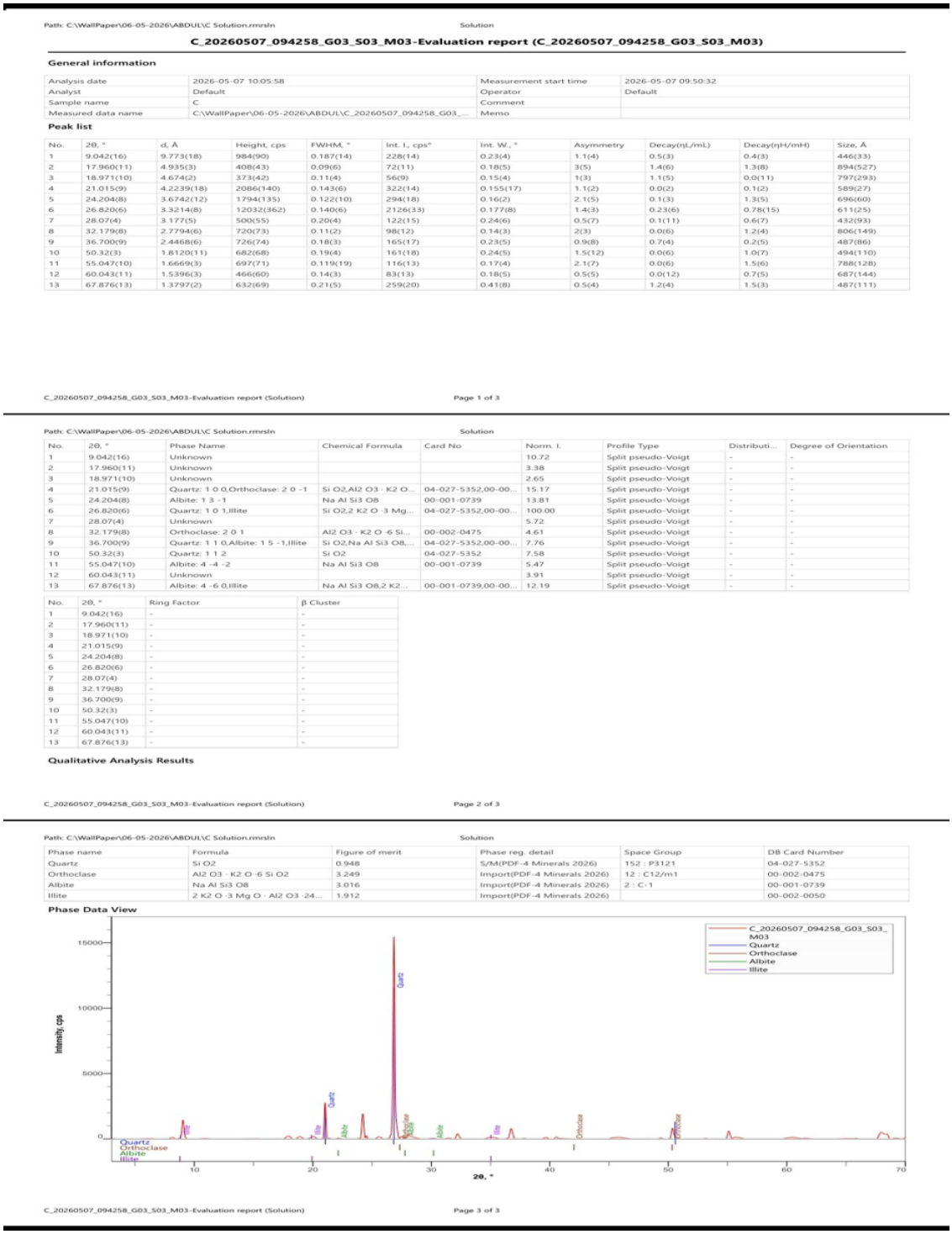

Path: C:\WallPaper\06-05-2026\ABDUL\C Solution.rmrsln Solution

C_20260507_094258_G03_S03_M03-Evaluation report (C_20260507_094258_G03_S03_M03)

General information

Analysis date	2026-05-07 10:05:58	Measurement start time	2026-05-07 09:50:32
Analyst	Default	Operator	Default
Sample name	C	Comment	
Measured data name	C:\WallPaper\06-05-2026\ABDUL\C_20260507_094258_G03_...	Memo	

Peak list

No.	2θ, °	d, Å	Height, cps	FWHM, °	Int. I., cps*	Int. W., °	Asymmetry	Decay(n)L/mL)	Decay(n)H/mH)	Size, Å
1	9.042(16)	9.773(18)	984(90)	0.187(14)	228(14)	0.23(4)	1.1(4)	0.5(3)	0.4(3)	446(33)
2	17.960(11)	4.935(3)	408(43)	0.09(6)	72(11)	0.18(5)	3(5)	1.4(6)	1.3(8)	894(527)
3	18.971(10)	4.674(2)	373(42)	0.11(4)	56(9)	0.15(4)	1(3)	1.1(5)	0.0(11)	797(293)
4	21.015(9)	4.2239(18)	2086(140)	0.143(6)	322(14)	0.155(17)	1.1(2)	0.0(2)	0.1(2)	589(27)
5	24.204(8)	3.6742(12)	1794(135)	0.122(10)	294(18)	0.16(2)	2.1(5)	0.1(3)	1.3(5)	696(60)
6	26.820(6)	3.3214(8)	12032(362)	0.140(6)	2126(33)	0.177(8)	1.4(3)	0.23(6)	0.78(15)	611(25)
7	28.07(4)	3.177(5)	500(55)	0.20(4)	122(15)	0.24(6)	0.5(7)	0.1(11)	0.6(7)	432(93)
8	32.179(8)	2.7794(6)	720(73)	0.11(2)	98(12)	0.14(3)	2(3)	0.0(6)	1.2(4)	806(149)
9	36.700(9)	2.4468(6)	726(74)	0.18(3)	165(17)	0.23(5)	0.9(8)	0.7(4)	0.2(5)	487(86)
10	50.32(3)	1.8120(11)	682(68)	0.19(4)	161(18)	0.24(5)	1.5(12)	0.0(6)	1.0(7)	494(110)
11	55.047(10)	1.6669(3)	697(71)	0.119(19)	116(13)	0.17(4)	2.1(7)	0.0(6)	1.5(6)	788(128)
12	60.043(11)	1.5396(3)	466(60)	0.14(3)	83(13)	0.18(5)	0.5(5)	0.0(12)	0.7(5)	687(144)
13	67.876(13)	1.3797(2)	632(69)	0.21(5)	259(20)	0.41(8)	0.5(4)	1.2(4)	1.5(3)	487(111)

C_20260507_094258_G03_S03_M03-Evaluation report (Solution) Page 1 of 3

Path: C:\WallPaper\06-05-2026\ABDUL\C Solution.rmrsln Solution

No.	2θ, °	Phase Name	Chemical Formula	Card No	Norm. I.	Profile Type	Distributi...	Degree of Orientation
1	9.042(16)	Unknown			10.72	Split pseudo-Voigt	-	-
2	17.960(11)	Unknown			3.38	Split pseudo-Voigt	-	-
3	18.971(10)	Unknown			2.65	Split pseudo-Voigt	-	-
4	21.015(9)	Quartz: 1 0 0,Orthoclase: 2 0 -1	Si O2,Al2 O3 · K2 O...	04-027-5352,00-00...	15.17	Split pseudo-Voigt	-	-
5	24.204(8)	Albite: 1 3 -1	Na Al Si3 O8	00-001-0739	13.81	Split pseudo-Voigt	-	-
6	26.820(6)	Quartz: 1 0 1,Illite	Si O2,2 K2 O ·3 Mg...	04-027-5352,00-00...	100.00	Split pseudo-Voigt	-	-
7	28.07(4)	Unknown			5.72	Split pseudo-Voigt	-	-
8	32.179(8)	Orthoclase: 2 0 1	Al2 O3 · K2 O ·6 Si...	00-002-0475	4.61	Split pseudo-Voigt	-	-
9	36.700(9)	Quartz: 1 1 0,Albite: 1 5 -1,Illite	Si O2,Na Al Si3 O8,...	04-027-5352,00-00...	7.76	Split pseudo-Voigt	-	-
10	50.32(3)	Quartz: 1 1 2	Si O2	04-027-5352	7.58	Split pseudo-Voigt	-	-
11	55.047(10)	Albite: 4 -4 -2	Na Al Si3 O8	00-001-0739	5.47	Split pseudo-Voigt	-	-
12	60.043(11)	Unknown			3.91	Split pseudo-Voigt	-	-
13	67.876(13)	Albite: 4 -6 0,Illite	Na Al Si3 O8,2 K2...	00-001-0739,00-00...	12.19	Split pseudo-Voigt	-	-

No.	2θ, °	Ring Factor	β Cluster
1	9.042(16)	-	-
2	17.960(11)	-	-
3	18.971(10)	-	-
4	21.015(9)	-	-
5	24.204(8)	-	-
6	26.820(6)	-	-
7	28.07(4)	-	-
8	32.179(8)	-	-
9	36.700(9)	-	-
10	50.32(3)	-	-
11	55.047(10)	-	-
12	60.043(11)	-	-
13	67.876(13)	-	-

Qualitative Analysis Results

C_20260507_094258_G03_S03_M03-Evaluation report (Solution) Page 2 of 3

Path: C:\WallPaper\06-05-2026\ABDUL\C Solution.rmrsln Solution

Phase name	Formula	Figure of merit	Phase reg. detail	Space Group	DB Card Number
Quartz	Si O2	0.948	S/M(PDF-4 Minerals 2026)	152 : P3121	04-027-5352
Orthoclase	Al2 O3 · K2 O ·6 Si O2	3.249	Import(PDF-4 Minerals 2026)	12 : C12/m1	00-002-0475
Albite	Na Al Si3 O8	3.016	Import(PDF-4 Minerals 2026)	2 : C-1	00-001-0739
Illite	2 K2 O ·3 Mg O · Al2 O3 ·24...	1.912	Import(PDF-4 Minerals 2026)		00-002-0050

Phase Data View

C_20260507_094258_G03_S03_M03-Evaluation report (Solution) Page 3 of 3

Figure 9. XRD evaluation report – Sample C (Scent leaf extract)

The XRPD data confirm that all three extracts are predominantly amorphous in character, as would be expected of complex, multi-constituent plant extracts, with varying degrees of crystalline mineral inclusion. The presence of silica polymorphs, potassium salts, and feldspathic minerals across the three samples is a natural consequence of the botanical and ecological origins of the plant materials. These findings are in agreement with recent characterization studies on comparable tropical medicinal plant extracts (Ndukwe *et al*., 2021; Chauhan *et al*., 2020; Onwudiwe *et al*., 2023).

Table 2. Summary of XRPD Quantitative Phase Analysis of the Three Plant Extracts

Sample	Identified Phases	Composition wt% (± uncertainty)	Dominant Phase
A – Bitter leaf	Urea, syn; Silvialite; Cristobalite; Sylvite	56(13); 13(3); 23(6); 8(22)	Urea, syn 56%
B – Neem leaf	Urea, syn; Sylvite; Graphite; Cristobalite; Marialite	16(28); 9(26); 21(44); 31(36); 22(51)	Cristobalite 31%
C – Scent leaf	Quartz; Orthoclase; Illite; Albite	64(4); 22(3); 11(3); 3(3)	Quartz 64%

Values in parentheses = standard uncertainties (wt%); database: PDF-4 Minerals 2026

Scanning Electron Microscope–Energy Dispersive X-Ray Analysis (SEM-EDX)

SEM-EDX combines high-resolution imaging of particle surfaces with element-specific X-ray detection, making it a particularly informative technique for characterizing the morphology and elemental composition of herbal extract particles intended for pharmaceutical use (Aulton and Taylor, 2021; Ibrahim *et al*., 2022). Analysis was conducted on the Phenom World SEM platform at 15 kV accelerating voltage using BSD Full detector, with a field of view of 537 µm and point-mode EDX acquisition. All three samples were analyzed in April 2026.

At% = Atomic concentration; Wt% = Weight concentration; EDX analysis performed at 15 kV, Phenom World SEM platform, April 2026.

Table 3. EDX Elemental Composition of the Three Plant Extracts (Atomic and Weight Concentrations)

Sample	Element	O At%	O Wt%	C At%	C Wt%	Other Elements	At%	Wt%
A – Bitter leaf	Detected	72.05	73.26	24.46	18.67	K, Si	2.62; 0.87	6.52; 1.55
B – Neem leaf	Detected	66.12	68.54	22.89	17.81	N, B, Ca, K	4.79; 3.56; 1.59; 1.06	4.35; 2.49; 4.12; 2.68
C – Scent leaf	Detected	68.56	69.20	19.29	14.61	N, B, K, Ca, Mg	3.96; 3.66; 1.85; 1.53; 1.16	3.50; 2.49; 4.56; 3.86; 1.78

Sample A- bitter leaf extract (*Vernonia amygdalina*) - displayed a highly heterogeneous surface morphology at all magnifications. The lower-magnification micrograph (Figure 10a) reveals a complex mixture of irregular flaky fragments, granular aggregates, and rounded particles packed together without a consistent size or shape distribution. At higher magnification (Figure 10b), the surface texture of individual particles becomes clearer, showing rough, pitted surfaces interspersed with smaller adhered microparticles - a morphological profile consistent with a dried, multi-component organic extract matrix that retains embedded crystalline mineral inclusions, as also indicated by XRPD analysis (Onwudiwe *et al*., 2023). The further high-magnification view (Figure 10c) reveals cracked, layered plate-like surfaces with what appear to be exposed internal fracture planes, consistent with brittle amorphous organic material.

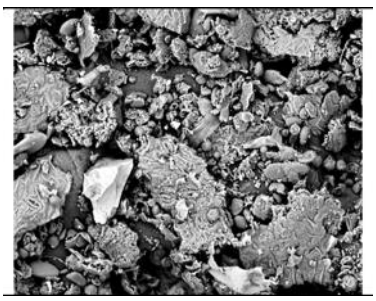

Figure 10a. SEM micrograph of Sample A (Bitter leaf extract)–lower magnification, showing heterogeneous particle morphology.

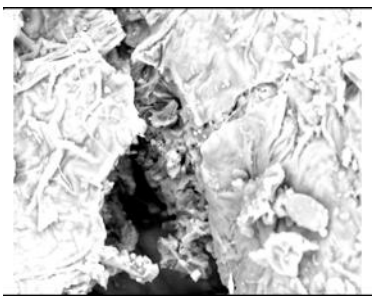

Figure 10b. SEM micrograph of Sample A (Bitter leaf extract)–higher magnification, showing rough particle surfaces with granular deposits.

Figure 10c. SEM micrograph of Sample A (Bitter leaf extract)–showing mixed flaky and granular fragments at higher magnification.

EDX elemental analysis of Sample A (Table 3), confirmed oxygen as the most abundant element at 72.05 atomic% (73.26 wt%), followed by carbon at 24.46 atomic% (18.67 wt%), potassium at 2.62 atomic% (6.52 wt%), and silicon at 0.87 atomic% (1.55 wt%). The dominant oxygen and carbon signals are consistent with the organic phytochemical matrix of the extract, comprising polyphenols, flavonoids, and terpenoids (Onwudiwe *et al*., 2023). The potassium signal provides direct elemental confirmation of the sylvite (KCl) phase identified by XRPD in this sample. Silicon, though at lower concentration, confirms the presence of silica phytoliths within the bitter leaf tissue, consistent with cristobalite identification in the XRD data (Ndukwe *et al*., 2021).

Notably, nitrogen was below the reliable EDX detection threshold in the analysis, though its presence is expected given the urea-syn phase predominance in the XRPD data; this discrepancy may reflect the inherent limitation of EDX for reliably quantifying light elements such as nitrogen (Ibrahim *et al*., 2022).

Sample B- *Neem* leaf extract (*Azadirachta indica*), exhibited a heterogeneous morphology, but with some features that distinguished it from the bitter leaf extract. The micrographs (Figures 11a–c) show a mix of flat plate-like fragments with a distinctive surface relief pattern alongside smaller irregular granules and spherical microparticles. The flat, layered plates observed are particularly characteristic of waxy or resinous phytochemical fractions, such as the triterpenoids and limonoids abundant in neem, which tend to crystallize or solidify into tabular habits upon drying (Siddiqui *et al*., 2022). The surface texture of many particles appears rougher and more granular at higher magnification, with extensive microparticle coverage of larger aggregate surfaces. This multi-scale particle organization reflects the complexity of the neem extract matrix, where organic phytochemical material, mineral phases, and dried essential oil residues co-exist within the same powder bulk.

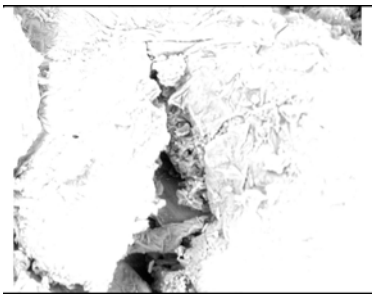

Figure 11a. SEM micrograph of Sample B (Neem leaf extract)–showing flat plate-like particles with irregular granular aggregates.

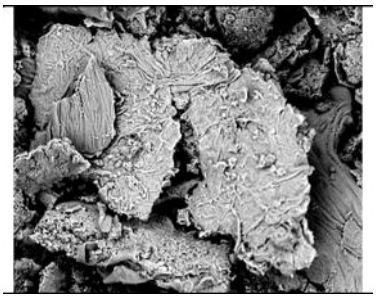

Figure 11b. SEM micrograph of Sample B (Neem leaf extract)–higher magnification showing surface texture and layered particle morphology.

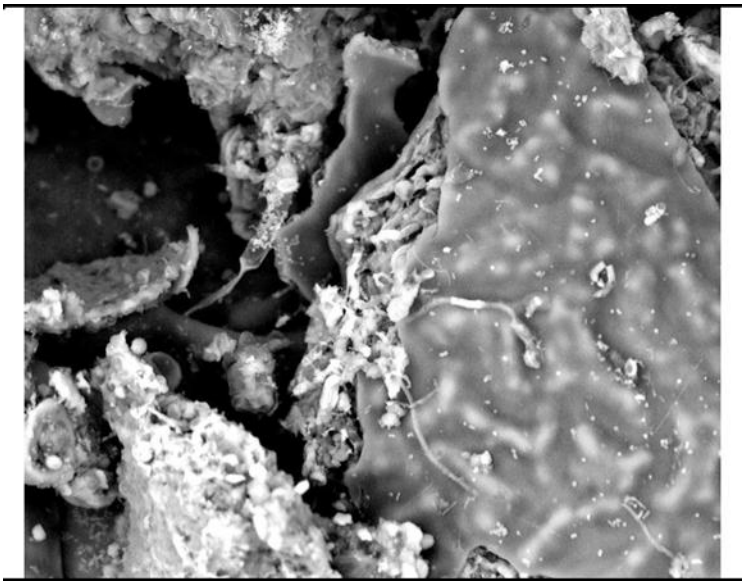

Figure 11C. SEM micrograph of Sample B (Neem leaf extract)–further magnification revealing surface microstructure and mineral inclusion deposits.

Sample C-Scent leaf extract (*Ocimum gratissimum*), displayed the most morphologically distinctive SEM profile of the three extracts. The micrographs (Figures 12a–c) reveal a mixture of smooth, flat plate-like fragments with well-defined edges alongside more irregular granular material. The large, smooth-surfaced plates with subtle surface relief are particularly striking and are consistent with the solidification of waxy cuticle material or essential oil concentrate upon drying. Interspersed with these smooth plates are more irregular, porous aggregates and smaller particles that appear to represent a different morphological component, likely the mineral-rich fraction predicted by the high quartz and feldspar XRPD result. At higher magnification, the surfaces of larger particles show fine surface corrugations, small adherent spherical microparticles, and occasional surface voids, reflecting the porous microstructure of dried plant cell wall fragments (Khalil *et al*., 2022; Ndukwe *et al*., 2021).

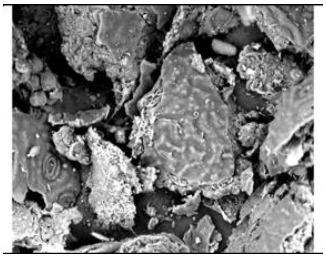

Figure 12a. SEM micrograph of Sample C (Scent leaf extract) overview showing smooth plate-like and irregular granular particle morphologies.

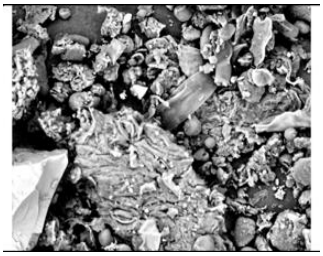

Figure 12b. SEM micrograph of Sample C (Scent leaf extract) at higher magnification showing smooth-surfaced plates alongside porous granular aggregates.

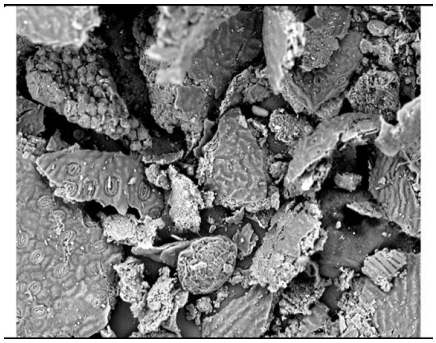

Figure 12C. SEM micrograph of Sample C (Scent leaf extract)–showing fragmented plate-like particles with surface microstructure details.

EDX elemental analysis of Sample C (Table 4.) showed oxygen at 68.56 atomic% (69.20 wt%) and carbon at 19.29 atomic% (14.61 wt%), with the lowest carbon content of the three samples. The elemental profile of scent leaf extract was the most complex and diverse: nitrogen was present at 3.96 atomic% (3.50 wt%), boron at 3.66 atomic% (2.49 wt%), potassium at 1.85 atomic% (4.56 wt%), calcium at 1.53 atomic% (3.86 wt%), and magnesium at 1.16 atomic% (1.78 wt%). The presence of magnesium is a notable feature unique to Sample C among the three extracts, and is consistent with the known role of magnesium as a component of chlorophyll in Lamiaceae species, as well as magnesium-containing mineral phases that may persist through the extraction process (Khalil *et al*., 2022). The elevated potassium concentration relative to the other samples aligns with *Ocimum gratissimum's* characteristically high potassium content documented in nutritional and phytochemical studies (Khalil *et al*., 2022). The calcium signal is consistent with calcium oxalate crystals and calcium-bound organic acids commonly found in Lamiaceae leaf extracts (Ibrahim *et al*., 2022). Collectively, the SEM-EDX data across all three samples provide direct visual and elemental confirmation of the physicochemical profiles established by DSC and XRPD, and offer additional insight into the particle-level characteristics that will influence the dispersion, texture, and stability of the final cream formulation (Aulton and Taylor, 2021).

Physicochemical properties of plants' extracts

The results of the physicochemical properties are summarized in Table 5.

Table 5. Physicochemical properties of the three plant extracts

Parameter	Neem Leaf Extract	Bitter Leaf Extract	Scent Leaf Extract
Colour	Dark greenish-brown	Dark green	Greenish-brown
Odour	Bitter, pungent	Bitter, characteristic	Aromatic, spicy
Texture	Amorphous solid	Amorphous solid	Amorphous solid
pH (1% w/v aqueous)	5.8 ± 0.12	6.1 ± 0.08	6.3 ± 0.10
Loss on Drying (%)	5.42 ± 0.32	4.87 ± 0.24	6.15 ± 0.41
Total Ash (%)	8.31 ± 0.15	10.42 ± 0.22	12.18 ± 0.31
Acid-insoluble Ash (%)	1.24 ± 0.08	1.08 ± 0.05	2.41 ± 0.12
Water-soluble Ash (%)	5.62 ± 0.19	7.14 ± 0.27	6.83 ± 0.18
Ethanol Extractive Value (%)	11.20 ± 0.45	9.30 ± 0.38	7.65 ± 0.29
Refractive Index	1.3842 ± 0.002	1.3761 ± 0.003	1.3795 ± 0.002
Solubility in Water	Partially soluble	Partially soluble	Partially soluble
Solubility in Ethanol	Freely soluble	Freely soluble	Freely soluble

Values represent mean ± SD (n = 3)

V. Conclusion

The findings of this research demonstrate that the ethanolic leaf extracts of *Azadirachta indica*, *Vernonia amygdalina*, and *Ocimum gratissimum* possess physicochemical characteristics that are important for pharmaceutical topical dosage development. Through the application of advanced analytical techniques such as DSC, XRPD, and SEM-EDX, valuable information was generated regarding the thermal behavior, structural properties, morphology, and elemental composition of the extracts. These investigations contributed significantly to understanding the nature of the plant materials and provided essential data that could support future formulation studies. The characterization results further emphasize the importance of comprehensive preformulation evaluation in the development of topical herbal medicinal products.

The findings suggest that neem, bitter leaf, and scent leaf contain bioactive constituents capable of inhibiting the growth of clinically relevant microorganisms. The data generated serve as a valuable foundation for future studies aimed at developing standardized topical herbal formulations and exploring the therapeutic potential of these plants in greater detail.

References

[1]. Kumar, S., Singh, J., And Sharma, A. (2020). Topical Drug Delivery Systems: A Review. Ku International Journal Of Pharmaceutical Sciences And Research, 11(7), 3021–3032.
[2]. Aulton, M. E., And Taylor, K. M. G. (2018). Aulton's Pharmaceutics: The Design And Manufacture Of Medicines (5th Ed.). Elsevier.
[3]. World Health Organization (WHO). (2023). Global Report On Traditional And Complementary Medicine. Geneva: WHO.
[4]. Subapriya, R., And Nagini, S. (2005). Medicinal Properties Of Neem Leaves: A Review. Current Medicinal Chemistry – Anti-Cancer Agents, 5(2), 149–156.
[5]. Farombi, E. O., And Owoeye, O. (2011). Antioxidative And Chemopreventive Properties Of Vernonia Amygdalina And Garcinia Biflavonoid. International Journal Of Environmental Research And Public Health, 8(6), 2533–2555. Https://Doi.Org/10.3390/Ijerph8062533
[6]. Prabhu, K. S., Lobo, R., Shirwaikar, A. A., And Shirwaikar, A. (2009). Ocimum Gratissimum: A Review Of Its Chemical And Pharmacological Properties. The Open Complementary Medicine Journal, 1, 1–15.
[7]. Naikwadi, S. P., And Bhise, K. S. (2023). Pharmacognostic Authentication And Standardisation Of Medicinal Plant Raw Materials: Current Perspectives. Journal Of Medicinal Plants Studies, 11(1), 21–29.
[8]. Azwanida, N. N. (2015). A Review On The Extraction Methods Use In Medicinal Plants: Principle, Strength And Limitation. Medicinal & Aromatic Plants, 4(3), 196. Https://Doi.Org/10.4172/2167-0412.1000196
[9]. Ncube, N. S., Afolayan, A. J., And Okoh, A. I. (2022). Assessment Techniques Of Antimicrobial Properties Of Natural Compounds Of Plant Origin: Current Methods And Future Trends. African Journal Of Biotechnology, 7(12), 1797–1806. Https://Doi.Org/10.5897/AJB08.030
[10]. World Health Organization (WHO). (2019). WHO Global Report On Traditional And Complementary Medicine 2019. Geneva: World Health Organization.
[11]. Edeoga, H. O., Okwu, D. E., And Mbaebie, B. O. (2020). Phytochemical Constituents Of Some Nigerian Medicinal Plants. African Journal Of Biotechnology, 4(7), 685–688. Https://Doi.Org/10.5897/AJB2005.000-3108
[12]. Mandal, S. C., Mandal, V., And Das, A. K. (2021). Essentials Of Botanical Extraction: Principles And Applications (2nd Ed.). Academic Press.
[13]. Pandey, A., And Tripathi, S. (2022). Concept Of Standardisation, Extraction And Pre-Phytochemical Screening Strategies For Herbal Drug Research. Journal Of Pharmacognosy And Phytochemistry, 3(5), 115–119.
[14]. Trease, G. E., And Evans, W. C. (2022). Trease And Evans' Pharmacognosy (17th Ed.). Elsevier Health Sciences.
[15]. Harborne, J. B. (2019). Phytochemical Methods: A Guide To Modern Techniques Of Plant Analysis (3rd Ed.). Springer Science & Business Media.
[16]. United States Pharmacopeia. (2023). USP 46–NF 41: General Chapters: Powder Flow. United States Pharmacopeial Convention.
[17]. Lachman, L., Lieberman, H. A., & Kanig, J. L. (2013). The Theory And Practice Of Industrial Pharmacy (4th Ed.). Varghese Publishing House.
[18]. Ogunjimi, A. T., Aworh, O. C., And Adeosun, S. A. (2022). Prevalence And Antibiotic Resistance Patterns Of Bacterial Isolates From Skin And Soft Tissue Infections In Southwest Nigeria. African Journal Of Clinical And Experimental Microbiology, 23(2), 180–191. Https://Doi.Org/10.4314/Ajcem.V23i2
[19]. Clinical And Laboratory Standards Institute. (2022). Methods For Dilution Antimicrobial Susceptibility Tests For Bacteria That Grow Aerobically (12th Ed.; CLSI M07-A12). CLSI.
[20]. Bhattacharyya, D. K. (2021). Research Methodology In Life Sciences (2nd Ed.). Academic Publishers.
[21]. Motulsky, H. J. (2021). Intuitive Biostatistics: A Nonmathematical Guide To Statistical Thinking (4th Ed.). Oxford University Press.
[22]. Siddiqui, B. S., Ahmed, F., Khan, S., Ahmad, A., And Sattar, S. A. (2022). Phytoconstituents And Biological Activities Of Azadirachta Indica A. Juss. (Neem): A State-Of-The-Art Review (2015–2021). Natural Product Research, 36(12), 3068–3085. Https://Doi.Org/10.1080/14786419.2021.1887538
[23]. Onwudiwe, N. N., Onyekwere, M. O., And Okorie, P. N. (2023). Quality Control Evaluation Of Vernonia Amygdalina Del. (Bitter Leaf) Extracts For Pharmaceutical Applications. African Journal Of Pharmacy And Pharmacology, 17(1), 1–10. Https://Doi.Org/10.5897/AJPP2022.5272
[24]. Khalil, O. A. K., Mohamed, E. A., Alrawabi, S. N., And Khalil, N. A. E. (2022). Phytochemical Profile And Biological Activities Of Ocimum Gratissimum: A Comprehensive Review. Natural Product Research, 36(8), 1939–1956. Https://Doi.Org/10.1080/14786419.2020.1839467
[25]. Azwanida, N. N. (2015). A Review On The Extraction Methods Use In Medicinal Plants: Principle, Strength And Limitation. Medicinal & Aromatic Plants, 4(3), 196. Https://Doi.Org/10.4172/2167-0412.1000196
[26]. Pandey, A., & Tripathi, S. (2014). Concept Of Standardization, Extraction And Pre-Phytochemical Screening Strategies For Herbal Drug. Journal Of Pharmacognosy And Phytochemistry, 2(5), 115–119.
[27]. Elufioye, T. O., Habtemariam, S., And Adejare, A. (2021). Chemistry And Pharmacology Of Alkenylphenols And Their Glycosides From Plants With Emphasis On Their Anti-Inflammatory And Antioxidant Activities. Revista Brasileira De Farmacognosia, 31(4), 396–413. Https://Doi.Org/10.1007/S43450-021-00164-5
[28]. Ruggiero, M. T., Zhang, W., Mittleman, A. G., And Zeitler, J. A. (2023). Predicting The Solubility Of Pharmaceutical Cocrystals Using Differential Scanning Calorimetry. Crystal Growth & Design, 23(4), 2718–2730. Https://Doi.Org/10.1021/Acs.Cgd.2c01489
[29]. Mura, P., Maestrelli, F., Cirri, M., And Mennini, N. (2022). Differential Scanning Calorimetry As A Screening Technique For Studying Drug–Excipient Interactions In Semi-Solid Formulations. Pharmaceutics, 14(3), 602. Https://Doi.Org/10.3390/Pharmaceutics14030602
[30]. Adetunji, C. O., Oloke, J. K., Kumar, A., Bhatt, P., And Swaranjit, S. C. (2021). Phytochemistry, Mode Of Action And Toxicity Of Some Essential Plant Extracts. Journal Of Natural Remedies, 21(1), 1–18. Https://Doi.Org/10.18311/Jnr/2021/26403
[31]. Chauhan, A., Lal, H., Bhatt, D. L., And Singh, P. (2020). Characterisation Of Herbal Raw Materials Using XRD Technique For Quality Assurance. Journal Of Pharmacognosy And Phytochemistry, 9(4), 1234–1241.
[32]. Ndukwe, K. C., Okeke, I. N., Lamikanra, A., Adesanya, S. A., And Ferne, M. (2021). Antimicrobial Activity And Mineral Content Of Selected Tropical Medicinal Plant Extracts. Journal Of Pharmacy And Pharmacology, 30(3), 1–9.
[33]. Farombi, E. O., & Owoeye, O. (2011). Antioxidative And Chemopreventive Properties Of Vernonia Amygdalina And Garcinia Biflavonoid. International Journal Of Environmental Research And Public Health, 8(6), 2533–2555. Https://Doi.Org/10.3390/Ijerph8062533